Waveform Design of UAV Data Links in Urban Environments for Interference Mitigation

Marko Jacovic, Oday Bshara, and Kapil R. Dandekar
Drexel University, Philadelphia, PA
Email: {mj355, ob67, krd26@drexel.edu}

***Abstract*—OFDM-based communication systems for Unmanned Aerial Vehicles (UAV) are designed predominately for high mobility scenarios with direct line of sight. The number of sub-channels used is selected to be small to mitigate the effects of inter-carrier interference (ICI) resulting from carrier frequency offset. We investigate interference effects in urban environments for quad-copter UAVs based on both ICI and inter-symbol interference (ISI), which results from multi-path scenarios. We propose that changing the number of sub-carriers used in the Air-to-Ground link improves bit error rate performance dependent upon the channel characteristics. In the presence of closely spaced buildings, a greater amount of multi-path will occur, motivating the use of more sub-carriers. A practical joint synchronizer is discussed to enable scalability of the proposed idea and characterize the source of ICI. Through the use of ray tracing models and realistic end-to-end simulations, we determine that UAV communications in urban environments benefit from adaptive sub-carrier counts to combat interference effects.**

***Index Terms*—Unmanned aerial vehicles, OFDM, Interchannel interference, Intersymbol interference, Channel models**

I. Introduction

UNMANNED Aerial Vehicles (UAVs) have the potential to solve many upcoming challenges in civil, industrial, and military domains due to flight speed capabilities, high maneuverability, and low-cost implementation. Applications may consist of disaster relief, data-collection, hot-spot base stations, and countless others. In each of the aforementioned scenarios it is vital that UAV communication systems are reliable and well protected [1]. Orthogonal Frequency Division Multiplexing (OFDM), a widely adopted multi-carrier transmission scheme, has been used in many wireless communication standards such as in IEEE 802.11, 3GPP Long Term Evolution, and WiMAX. In addition, OFDM was used for UAV communication in the Broadband Aeronautical Multi-Carrier System, and is the focus of the current emerging standard L-Band Digital Aeronautical Communications Systems 1 (LDACS1) [2].

In contrast to single-carrier wide-band modulation schemes, OFDM uses a large number of parallel narrow-band sub-carriers and does not require additional frequency guard-bands between sub-carriers. As a result, OFDM efficiently compensates for multi-path effects and is robust against narrow-band interference; however, it suffers from high peak-to-average-power ratio, phase noise effects, and sensitivity to Carrier Frequency Offset (CFO) [3]. CFO is attributed to either a mismatch between local oscillators or from doppler shift due to node mobility. Severe performance degradation results from CFO due to the loss of orthogonality between sub-carriers, leading to a phenomenon known as Inter-Carrier Interference (ICI). Frequency acquisition algorithms are implemented at receivers to mitigate the effects of CFO; however, ICI from external sources or from estimation error may still be prevalent [4]. Under high mobility it is necessary for OFDM signals to have a lower number of sub-channels to tolerate the resulting ICI effects [5] [6].

The selection of the number of sub-carriers used for an OFDM signal under a fixed bandwidth is a two-dimensional consideration. As the number of sub-carriers is made smaller, the frequency spacing will be larger and the system will be more resilient of ICI; however, as the number increases, the signal bandwidth of each sub-carrier becomes smaller relative to the coherence bandwidth of the channel and the system becomes more tolerant to Inter-Symbol Interference (ISI). OFDM systems with adaptive sub-carrier spacing have been shown to yield capacity performance gains in the presence of ICI and in low received signal power scenarios in [7]. The authors did not consider ISI channels or the application of adaptation for UAVs, in particular for rotary types which due not travel and hundreds of km/h as in their study. Previous work has been done in mitigating ICI for OFDM-based UAV communications based on computationally complex channel estimation procedures, but lacked discussion of synchronization and realistic channel modeling [8]. Additional analysis has been performed to integrate UAV systems into LTE, although these studies focused on open-field scenarios [9].

In all the aforementioned studies, the only impairment that was considered to have a strong impact on UAV communications was ICI. Dense urban environments may result in multi-path effects due to obstructions in the propagation path, leading to ISI [3]. The type of UAV used in Air-to-Ground (A2G) communication must be in consideration. A fixed-wing UAV is capable of traveling at high speeds but unable to hover, while in direct contrast, a rotary based UAV is able to maneuver with a much finer degree of control but is unable to meet the same velocity [1]. The behavior of the UAV and its propagation environment must be regarded in waveform design.

In this paper, we examine the characteristics of an A2G channel in an urban environment to demonstrate that a performance gain is achieved from an increase in sub-channels in multi-path scenarios. We provide practical synchronization methods that support different FFT sizes and discuss their

effect on ICI. We argue that further considerations for the number of OFDM sub-channels needs to be made based on UAV target applications. In addition, our findings motivate future studies for waveform adaptation techniques based on system feedback. The contribution of this paper is in analyzing the tradeoffs of OFDM waveform design against interference, in particular ISI, for rotary-based UAVs in urban environments. The remainder of this document is as follows: in Section II an overview of the communication system and distortion effects are presented, a description of our channel model is provided in Section III, the synchronization algorithm used is described in Section IV, system evaluation is evaluated in Section V, and concluding remarks are offered in Section VI.

II. System Model and Problem Description

In this study, we consider an OFDM-based communication link between an in-air UAV and a ground user in an urban environment. The link experiences effects related to interfering objects, mobility, and RF front-end distortions. Mismatch of local oscillators (LO) and Doppler shift due to mobility lead to CFO. The amount of CFO in Hz is given as

$$f_d = \frac{v}{\lambda} + \psi \tag{1}$$

where v is the velocity of the UAV in m/s, λ is the signal wavelength in m, and ψ is the offset due to the LO mismatch. The value of ψ is randomly distributed based on the design specifications of the LO error in ppm and the signal carrier frequency. The received signal through the channel with additional effects may be expressed as

$$y[n] = h[n] * x[n] e^{\frac{j2\pi\nu n}{N}} + z[n] \tag{2}$$

where $h[n]$ is the channel impulse response, $x[n]$ is the transmitted OFDM signal, ν is the CFO relative to the sub-carrier spacing, N is the number of sub-channels, and $z[n]$ is a noise component. The channel characteristics are based on the surrounding environment of the link, which is an important consideration in the presence of buildings and other objects. A detailed discussion of our UAV A2G channel model $h[n]$ is provided in the next section. CFO results in ICI as the orthogonality between OFDM sub-carriers will be lost. Frequency synchronization is used at the receiver to correct for the offset and reduce the effects of ICI. Due to the trade-offs between latency, complexity, and performance, residual error will exist after synchronization. In addition, the CFO acquisition range is limited to a design parameter for practical implementations. Both of these errors become more detrimental as the frequency separation of the sub-carriers decreases. Considering a limited signal bandwidth, in scenarios where ICI is considered the dominant effect, it is advantageous to maximize the sub-carrier spacing by selecting a lower number of OFDM sub-channels, N. A key advantage of using a larger number of sub-carriers is increased robustness to multi-path environments, as each sub-channel undergoes flat instead of frequency-selective fading. Large delay spread of the channel results in ISI. The cyclic prefix length is selected to combat the effects of ISI, by turning the linear convolution of the OFDM signal with the channel into a circular convolution, enabling simple frequency domain equalization. Temporal efficiency is reduced as the length of the cyclic prefix increases. In both ICI and ISI the system performance is degraded; however, studies to date have focused primarily on the effects of ICI in the domain of UAV communication [5] [6] [8]. Further studies could be performed to modify the cyclic prefix size and Quadrature Amplitude Modulation (QAM) order as well to yield performance gains under different conditions, but these parameters are considered fixed in our study. In this work we focus on the benefit of using different number of sub-carriers to combat different types of interference conducive to urban UAV A2G communication.

III. Channel Model

Ray tracing is used to analyze propagation environments where actual measurements are difficult to acquire due to frequency licensing or equipment cost. In addition, ray tracing is used during proof of concept analysis where simulation data sets are consumed by analytic processing models [10]. In this paper we use the Wireless Insite software package from Remcom company to collect our channel measurements. Wireless InSite applies physics driven propagation models to a specific indoor or outdoor environment based on buildings, material, waveform, antennas, and transmitter (Tx) and receiver (Rx) locations [11]. We use complex impulse responses for each path of propagation between every Tx-Rx link with corresponding delay spread in our study [12]. The time of arrival for each propagation path is given by:

$$t_i = \frac{L_i}{c} \tag{3}$$

where L_i is the total geometrical path length, and c is the speed of light in free space. The mean time of arrival is:

$$\bar{t} = \frac{\sum_{i=1}^{N_P} P_i t_i}{P_R} \tag{4}$$

where P_R is the average received power, P_i is the time average power in watts of the i^{th} path. The delay spread is a power-weighted root mean square of the time delays, calculated assuming a narrow-band signal at the carrier frequency by:

$$\sigma = \sqrt{\frac{\sum_{i=1}^{N_P} (t_i - \bar{t})^2 P_i}{P_R}} \tag{5}$$

In our study a rotary-based UAV hovers around Drexel University concrete buildings in the University City campus in Philadelphia as shown in Figure 1 at a height of 25m with a speed that introduces Doppler frequency shift at the receiver. The complex impulse response has been collected at different links between an Rx placed 2m above the ground and the UAV Tx at 3m spaced positions of its route as shown in Figure 2.

IV. Synchronization Mechanisms

Both timing and frequency synchronization are important aspects of any communication system, in particular for the purpose of understanding interference effects in UAV communications. ICI occurs from error of the CFO estimate attributed to LO mismatch and high mobility of UAVs, even if the

Fig. 1: Google Earth image of Drexel University campus area.

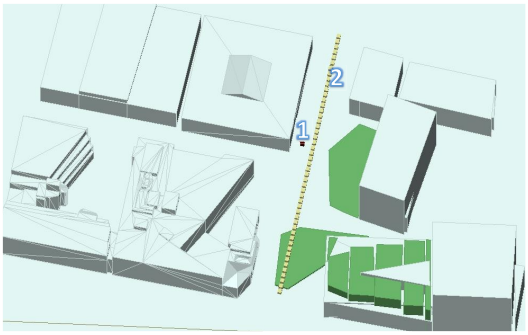

Fig. 2: Simulation model of Drexel University study area with (1) Ground Rx and (2) Tx along UAV route.

offset is within the acquisition range. The low-cost devices used in UAV communications have higher LO fluctuation, leading to CFO. Incorrect timing alignment and multi-path effects inherent in an urban environment may lead to ISI. In addition, the synchronizer used needs to be compatible with the proposed method of changing the number of sub-channels. The method selected for this work is primarily based on the Schmidl and Cox (S&C) algorithm from [4], due to its wide adoption and influence in the field. The key adjustments to the algorithm are filtering of the timing metric and the fine timing technique. We use a synchronizer designed for 64 sub-channels, regardless of the value of N for the payload symbols. A common preamble allows for practical system scalability for multiple communication links, since header fields may be used to decode payload parameters upon acquisition. In addition, this restriction ensures that a standard comparison of CFO error is considered, since a larger preamble size improves CFO estimation. Coarse timing is performed based on S&C with modifications, fractional and integer CFO estimation are implemented according to the original method, and fine timing is performed using cross-correlation.

A. Preamble Structure

The preamble used follows the design from S&C, consisting of 2 OFDM symbols. The first symbol in the frequency domain consists of a complex pseudonoise (PN) sequence of Quadrature Phase Shift Keying (QPSK) symbols on even sub-carriers and zeros on the odd sub-carriers. In the time-domain the first symbol consists of 2 identical repeated sequences. The second symbol is composed of two separate PN sequences. On the even sub-carriers, a sequence is selected such that a differentially modulated PN sequence may be calculated as a ratio of the even sub-carriers on the second and first symbols. The odd sub-carriers of the second symbol consist of an arbitrary PN sequence which serve the purpose of ensuring that the second symbol in time-domain does not exhibit a repetitive structure which may result in an increase of false positive errors during coarse timing synchronization.

B. Coarse Timing

The timing algorithm relies on a modified auto-correlation described by:

$$P[n] = \sum_{d=0}^{L-1} y^*[n+d]y[n+d+L] \tag{6}$$

where L is the length of the repeated sequence in the first training symbol, y is the received signal, and $(^*)$ represents the complex conjugate operation. Correlation provides a quantitative measure of similarity. Modifying the equation to advance the frame by L samples takes advantage of the repetitive structure of the first training symbol, as the maximum value of $P[n]$ will determine the starting point of the signal. The received energy of the second half of the first symbol is calculated as:

$$E[n] = \sum_{d=0}^{L-1} |y[n+d+L]|^2 \tag{7}$$

which allows for the timing metric to be a normalized quantity. The classical timing metric suffers from a significant plateau effect which influenced the authors in [13] to implement a metric filtered by the cyclic prefix length C. In our work, we use the modified timing metric

$$\Lambda[n] = \frac{1}{2C} \sum_{l=0}^{2C-1} \frac{|P[n-1]|^2}{E[n-l]^2} \tag{8}$$

with a window of $2C$ samples to reduce the influence of noise. The trajectory of the metric is not as sharp as a result; however, the inclusion of a fine timing mechanism compensates for the variance in coarse acquisition. The coarse timing point is selected at the maximum output of (8) offset by the length of the window.

C. Frequency Synchronization

Correction of CFO ν is a two stage process; requiring both fractional and integer values to be estimated for compensation of the received signal. The first symbol of the preamble is used to estimate the fractional frequency offset as:

$$\hat{\phi} = \frac{\angle P[\theta]}{2\pi} \tag{9}$$

where $P[\theta]$ is calculated from (6) at the acquired timing point θ. Correction is then be performed by multiplying the received signal by $e^{\frac{-j2\mathbf{n}\hat{\phi}}{N}}$, with $\mathbf{n}$ being a time vector. The fractional offset must be removed prior to integer offset estimation due to the effects of adjacent carrier interference. Integer CFO is determined by selecting frequency shift g which maximizes:

$$I[g] = \frac{|\sum_k x_1^*[k+g]\delta_k^* x_2[k+g]|^2}{2(\sum_k |x_2[k]|^2)^2} \tag{10}$$

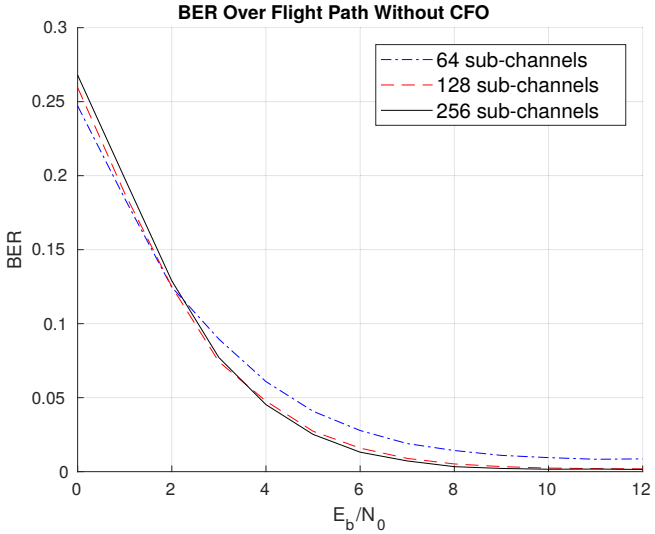

Fig. 3: BER comparison of N across flight path without CFO.

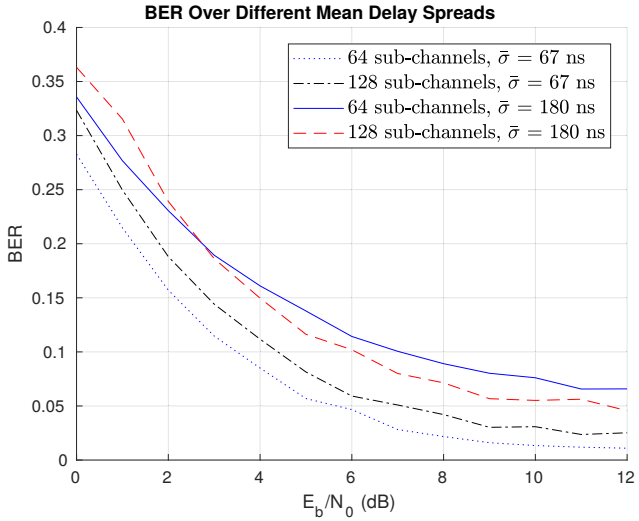

Fig. 4: BER comparison of N over mean delay spreads.

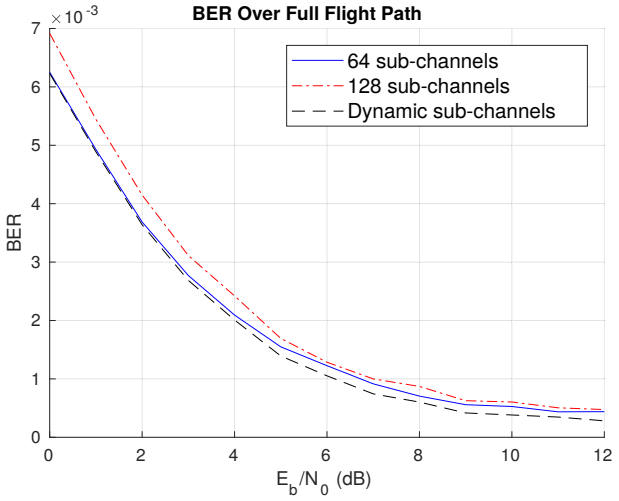

Fig. 5: BER comparison of N across entire flight path.

where k is the sub-carrier index constrained to N, x_1 is the first preamble symbol in frequency domain, x_2 is the second preamble symbol in frequency domain, and δ is the differentially modulated PN sequence. The metric may be interpreted as an exhaustive search of circular shifts of the received preamble in frequency domain to a known reference signal δ. The acquisition range of g is limited by a design parameter with the clear trade-offs of added computational complexity and latency. Correction to the signal is performed by multiplying the fractional CFO corrected signal by $e^{\frac{-j2\mathbf{n}\pi\hat{g}}{N}}$.

D. Fine Acquisition

Coherent cross-correlation may be used for improved timing acquisition, as a matched filter is the optimum receiver. Cross-correlation by itself fails due to significant CFO and must be implemented with coarse timing and frequency synchronization techniques for a reliable system as described in [14]. Fine timing is found by the cross-correlation

$$F[\tau] = \sum_{m=0}^{2(N+C)} y_{corr}[m+\tau]S^*[m] \tag{11}$$

where y_{corr} is the coarsely-timed frequency corrected received signal and $S[n]$ is the reference signal known to the receiver. The correlation is limited to two lengths of the preamble to reduce computational complexity. The delay τ that maximizes the absolute value of (11) is added to the coarse timing point to determine the final alignment of the synchronized signal. Fine CFO synchronization is performed by recalculating (9) and (10) at the fine timing point.

V. Performance Evaluation

In this section, the effect of varying the number of sub-channels used in an OFDM based UAV Air-to-Ground data link was examined through simulation. A carrier frequency of 1 GHz was selected with 20 MHz of bandwidth. Forward error correction was not implemented, and QPSK was used for single-carrier modulation to isolate the effect of N. The number of pilot tones used for phase tracking was set to $1/16$ of N, with equal spacing. The cyclic prefix was set to 16 for all values of N. Although a practical system may scale the cyclic prefix accordingly with the FFT size, the effects of ISI would be directly designed for at the expense of temporal inefficiency. The preamble was set for all values of N to be designed for 64 sub-carriers for the methods described in Section IV with a maximum CFO estimation range of $\pm 5g$. Increasing the FFT size of the training symbols also reduces the CFO estimation error, the key source of ICI, at the expense of added overhead. The CFO was applied to both preamble and payload samples in proportion to N, without biasing. To maintain a fair comparison of the effects of changing the number of sub-channels without ignoring related trade-offs, the aforementioned parameters were static. A minimum mean square error equalizer was used at the receiver based on two training symbols, with signal to noise ratio knowledge within ± 1 dB according to a uniform distribution of the actual value.

The channel modeling was performed using the method described previously in Section III. The UAV followed the flight path shown in Figure 2, and the ground terminal had a height of 2 meters. CFO was determined to be based predominately on the LO mismatch component in (1). The

value of ψ was selected from a random uniform distribution according to ± 20 ppm, which corresponds to a maximum theoretical shift of $\pm$ 40 kHz at the carrier frequency. The velocity was varied for difference scenarios, but noted to be negligible in comparison; a high speed such as 300 m/s corresponds to a shift of 1 kHz. At each data point of the flight path, the transmitted OFDM signal was convolved with the corresponding channel impulse response from the ray tracing model, then shifted in frequency according to velocity of 5 m/s and random LO offset. The velocity was selected as the maximum realistic speed of a rotary UAV. Noise was added to evaluate Bit Error Rate (BER) over normalized signal to noise ratio (SNR). The synchronizer was used at the receiver for practical evaluation and residual CFO effects. Multiple repeated trials were performed at each channel response to develop performance curves.

Different values of N were compared through the entirety of the flight path over varying $\frac{E_b}{N_0}$ without the presence of CFO in the system in Figure 3. Removal of CFO in this study highlighted the effects of ISI from the channel, and the results demonstrate that an increase in N yielded better performance. In Figure 4 the BER for 64 and 128 sub-carriers are compared for cases of strong Line of Sight (LOS) and multi-path conditions during the flight path. The LOS dominant channels had a mean delay spread of 67 ns. In these scenarios the effect of ICI was more prevalent, since there was minimal ISI, leading to the smaller FFT size of 64 performing better than 128. The multi-path channels, caused by reflections from nearby buildings, had a mean delay spread of 180 ns. In these cases the ISI effects were stronger and were more detrimental to the performance than ICI, therefore the BER decreased with 128 sub-channels used over 64. The increase in BER under 2 dB $\frac{E_b}{N_0}$ is due to synchronization error, in which smaller sub-carrier spacing is more susceptible to the effects. More complex synchronization algorithms may be implemented to overcome the degradation, if communication is desired in these very low SNR ranges. A comparison of using 64, 128, and dynamic selection of sub-carriers during the flight path is shown in Figure 5. The dynamic selection was based on known channel delay spread. The performance of 64 sub-carriers is marginally better than for 128 during this flight path, but the dynamic selection of N was shown to yield a performance gain. The results presented in this paper motivate the need for automated selection of the number of sub-carriers to combat interference effects in UAV data links. Future extensions of this work are focused on adaptation of waveform parameters using features derived from synchronization and channel estimation algorithms to improve system performance. Properties considered are number of sub-channels, as well as cyclic prefix length, and QAM order. Policy selection based on features such as estimated CFO, cross-correlation profile, and estimated delay spread will be explored.

VI. Conclusion

In this paper, we discussed the existence of both ICI and ISI effects in UAV data link communication. In contrast to previous approaches, we considered increasing the OFDM FFT size to improve system performance. Synchronization techniques were discussed to understand the sources of interference, and to ensure that the system is capable of being scaled for multiple link implementations. Realistic end-to-end simulations of Air-to-Ground channels created from ray tracing tools were performed for an urban environment with practical synchronization requirements and LO effects. Dominant LOS channels were shown to perform better with smaller FFT sizes, while links using a higher FFT size yielded better performance in multi-path channels, which are prevalent in urban settings. Overall it was shown that there is benefit to increasing the number of sub-channels used in UAV A2G communication links, instead of only designing against ICI.

Acknowledgment

This project is supported by the National Science Foundation through grant number CNS-1422964. We thank Alex Lackpour for his assistance with channel modeling and Simon Begashaw for his helpful suggestions on the paper.

References

[1] Y. Zeng, R. Zhang, and T. J. Lim, "Wireless communications with unmanned aerial vehicles: opportunities and challenges," *IEEE Communications Magazine*, vol. 54, no. 5, pp. 36–42, May 2016.

[2] R. Jain and F. Templin, "Requirements, Challenges and Analysis of Alternatives for Wireless Datalinks for Unmanned Aircraft Systems," *IEEE Journal on Selected Areas in Communications*, vol. 30, no. 5, pp. 852–860, June 2012.

[3] S. Haykin, *Digital Communication Systems*. Wiley, 2013.

[4] T. M. Schmidl and D. C. Cox, "Robust frequency and timing synchronization for OFDM," *IEEE Transactions on Communications*, vol. 45, no. 12, pp. 1613–1621, Dec 1997.

[5] V. Vahidi and E. Saberinia, "Orthogonal frequency division multiplexing and channel models for payload communications of unmanned aerial systems," in *2016 International Conference on Unmanned Aircraft Systems (ICUAS)*, June 2016, pp. 1156–1161.

[6] Z. Wu, H. Kumar, and A. Davari, "Performance evaluation of OFDM transmission in UAV wireless communication," in *Proceedings of the Thirty-Seventh Southeastern Symposium on System Theory, 2005. SSST '05.*, March 2005, pp. 6–10.

[7] S. S. Das, E. D. Carvalho, and R. Prasad, "Variable sub-carrier bandwidths in ofdm systems," in *2007 IEEE 65th Vehicular Technology Conference - VTC2007-Spring*, April 2007, pp. 1866–1870.

[8] V. Vahidi and E. Saberinia, "OFDM for payload communications of UAS: channel estimation and ICI mitigation," *IET Communications*, vol. 11, no. 15, pp. 2350–2356, 2017.

[9] I. Kovacs, R. Amorim, H. C. Nguyen, J. Wigard, and P. Mogensen, "Interference Analysis for UAV Connectivity over LTE Using Aerial Radio Measurements," in *2017 IEEE 86th Vehicular Technology Conference (VTC-Fall)*, Sept 2017, pp. 1–6.

[10] O. Bshara, Y. Liu, S. Begashaw, and K. R. Dandekar, "Computational Electromagnetic Simulation and Performance Analysis of Reconfigurable Antennas for Outdoor 60 GHz Applications," in *2017 IEEE Radio and Wireless Symposium (RWS)*, Jan 2017, pp. 38–41.

[11] P. Medeovi, M. Veleti, and . Blagojevi, "Wireless insite software verification via analysis and comparison of simulation and measurement results," in *2012 Proceedings of the 35th International Convention MIPRO*, May 2012, pp. 776–781.

[12] "Wireless Insite Propagation Software, Reference Manual," https://www.remcom.com/wireless-insite-em-propagation-software.

[13] H. Minn, M. Zeng, and V. K. Bhargava, "On timing offset estimation for OFDM systems," *IEEE Communications Letters*, vol. 4, no. 7, pp. 242–244, July 2000.

[14] A. B. Awoseyila, C. Kasparis, and B. G. Evans, "Robust time-domain timing and frequency synchronization for OFDM systems," *IEEE Transactions on Consumer Electronics*, vol. 55, no. 2, pp. 391–399, May 2009.